JOURNAL OF THERMOPHYSICS AND HEAT TRANSFER
Vol. 16, No. 3, July–September 2002

Highly Expanded Flashing Liquid Jets

J. R. Simões-Moreira,* M. M. Vieira,† and E. Angelo†
Universidade de São Paulo, 05508-900 São Paulo, Brazil

Results are presented of experiments with highly expanded flashing liquid jets along with a one-dimensional numerical model. The experiments were carried out with liquid iso-octane jets issuing from a small conical convergent nozzle into a low-pressure chamber. Images of the expanding jet off the nozzle exit section were obtained from a schlieren setup using a charge-coupled device camera. Analyses of these images enabled a qualitative visualization of the flashing jet structure and geometry. At very low backpressures, it has been observed that the emerging jet was formed by a central liquid core, and the phase change process occurred on the surface of that liquid core, giving rise to a sonic two-phase flow. In addition, it is also inferred that the freshly formed two-phase flow proceeded further to higher velocities and Mach numbers to terminate eventually with a complex shock wave structure to adjust pressures, as usual. A one-dimensional numerical analysis is carried out. The sudden phase change in the metastable liquid jet surface is modeled as an evaporation wave, for which the jump equations are solved. Next, the supersonic expansion of the two-phase mixture downstream of the evaporation wave is analyzed in a radial direction. The one-dimensional calculation yielded the radial position of the shock wave location. It has been found that the numerical results are consistent with the experimental data.

Introduction

IN some situations, a pressurized liquid may suddenly be exposed to a low-pressure environment. If the environmental pressure is somewhat lower than the corresponding saturation pressure, the liquid will undergo a fast phase transition process, commonly known as liquid flashing.

Liquid flashing studies are relevant to a multitude of industrial and technological fields. As examples, one can mention the following: 1) Disastrous industrial accidents have occurred as a consequence of rupturing a pressurized liquefied gas storage tank. In the literature, this phenomenon is known as boiling liquid expanding vapor explosion.[1] 2) The liquid fuel preheating process[2] has been investigated as a method of increasing fuel atomization for improvement of fuel injector technology. 3) Flashing mechanisms occurrence in expansion devices of refrigeration cycles have been studied,[3] which may be a source of intense noise. 4) In the 1960s and 1970s, the nuclear industry provided motivation for the study of the flashing phenomenon as it could occur in case of rupture[4] of pressurized water pipes. 5) Other applications include seawater desalination processes and flashing liquid jet analyses,[5,6] in a more fundamental sense.

The experiments were carried out with liquid iso-octane (C_8H_{18}) jets issuing from a small conical convergent nozzle into a low-pressure chamber. Photographic documentation revealed the existence of three liquid jet regimes: 1) continuous, 2) partially atomized, and 3) abrupt liquid evaporation with a two-phase supersonic expansion usually terminated by shock waves. Regime 1 occurred at backpressures above the vapor pressure at the initial testing temperature, so that no evaporation would occur. Regime 2 occurred at intermediate backpressure values. In the last situation, at very low backpressures (case 3), it has been inferred from photographic documentation[6–9] (also Figs. 1–4) that no phase transition or nucleation sites are observed in the liquid jet at the exit plane of the nozzle. Examination of still pictures taken using different photographic techniques[6–9] at a high shutter speed allows one to conclude that the jet emerging from the nozzle remains in the liquid phase. In addition, a liquid core is usually visible down to several nozzle diameters, whereas flashing takes place on the surface of this liquid core. With the usual assumption of incompressible flow, the simplified version of Bernoulli's equation along with the measured mass flow rate implies that the emerging liquid must be highly superheated or metastable at the nozzle exit section, that is, the liquid state has entered deeply into the metastable region. This description is valid for a low chamber pressure, that is, a backpressure value substantially below the saturation pressure corresponding to the initial injection temperature.

The main reason for working iso-octane is related to its retrograde behavior, which means that a high degree of evaporation can be reached during a liquid flashing process. As a consequence, retrograde substances are quite suitable for documenting flashing liquid experiments because a less dense cloud of droplets should surround the metastable liquid core, which evidently allows better and clearer pictures. A proper discussion of the retrograde behavior may be found in Refs. 10–12.

According to experimental data on mass flow measurements, choking-type behavior is observed as the backpressure is decreased, while keeping the liquid injection conditions unchanged (also see Fig. 5). This brings up a puzzling question: Why does the flow become choked if (metastable) liquid phase emerges from the nozzle? It is well known that the speed of sound in liquids is far greater than that of vapors and gases and that the liquid cannot become easily choked, except at extremely high injection pressures, neither of which occurred in the aforementioned experiments nor in those discussed in this paper.

Based on experimental observations, this paper contributes to elucidating the flashing liquid jet problem. The present findings of a metastable liquid jet emerging from the nozzle corroborate the work carried out by previous researchers (see Refs. 5–8, among others). The exiting jet comprises a liquid core from which a high-speed two-phase flow originates. Also, the metastable two-phase flow transition region is circumscribed by an interface that surrounds that metastable liquid core. This interface has been well studied using the concept of evaporation waves, which are phase change discontinuities similar to deflagration waves in a combusting gas.[7,10,11,13] The evaporation wave theory leads to a distinctive solution called the Chapman–Jouguet (C–J) point. As is well known, the C–J solution means that the two-phase flow is sonic in relation to the evaporating interface.

Received 4 June 2001; presented as Paper 2001-3036 at the AIAA 31st Fluid Dynamics Conference, Anaheim, CA, 11–14 June 2001; revision received 26 February 2002; accepted for publication 28 February 2002.

*Professor, Escola Politécnica, SISEA—Alternative Energy Systems Laboratory, Mechanical Engineering Department, P.O. Box 61548; jrsimoes@usp.br.

†Doctoral Student, Escola Politécnica, SISEA—Alternative Energy Systems Laboratory, Mechanical Engineering Department, P.O. Box 61548.

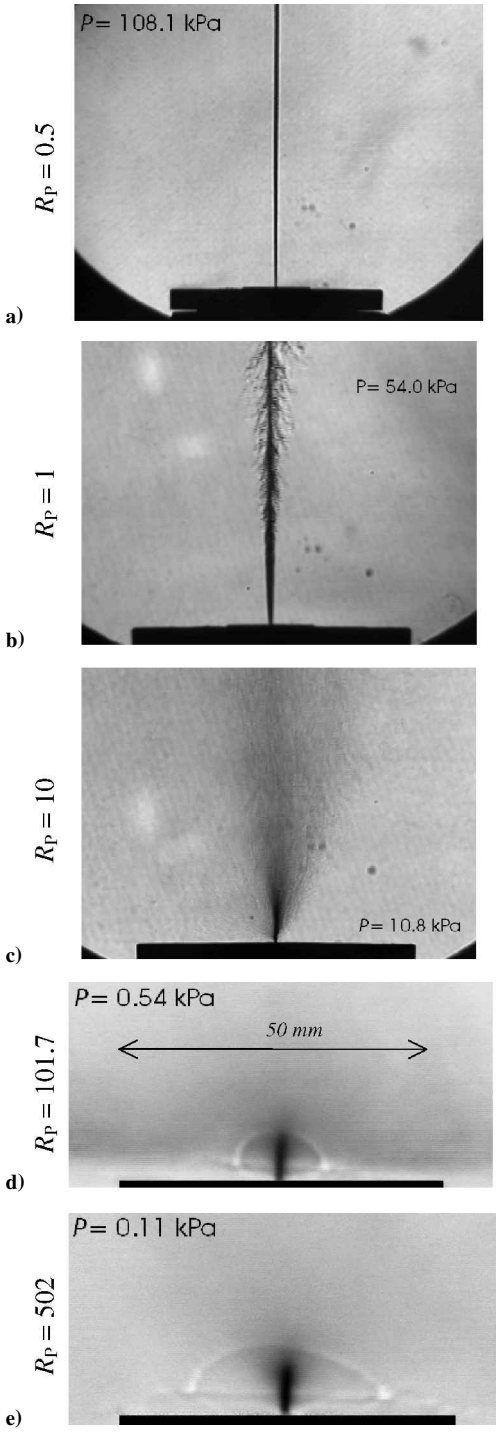

Fig. 1 Test series, nominal injection values $P_0 = 250$ kPa and $T_0 = 76°$C: from panel a to panel e, backpressure decreases (R_P increases). See Table 1 for measured data.

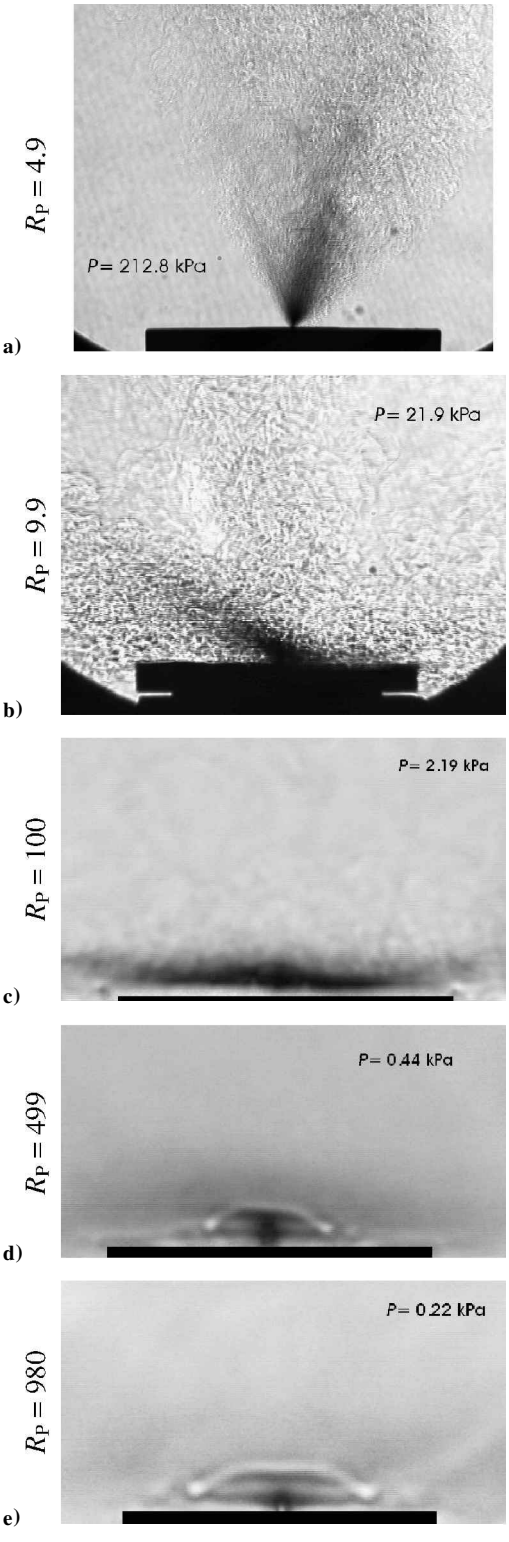

Fig. 2 Test series, nominal injection values $P_0 = 250$ kPa and $T_0 = 130°$C: from panel a to panel e, backpressure decreases (R_P increases). See Table 1 for measured data.

Other important questions that come out from the photographic documentation are associated with those observations that employed schlieren photographic techniques[8,9] (also Figs. 1–4) and optical interferometry.[7] Accordingly, a shock wave is sometimes seen coupled with the flashing liquid jet. This strongly indicates that a supersonic, or possibly a hypersonic, two-phase flow is present. This experimental observation corroborates the C–J solution, that is, the phase transition occurs at the metastable liquid core surface leading to the C–J solution, then the freshly formed sonic two-phase flow undergoes a free expansion process to increasing flow velocities and Mach numbers, which will terminate with shock wave structures to adjust pressures.

The next section describes the apparatus and experimental procedure. Experimental results are presented in the ensuing section. Then one-dimensional study is presented, including the theory of evaporation waves, the jump equations, and the conservation equations in the radial spherical coordinate form. Next, the results of the numerical solution and their analyses are presented. Finally, the paper finishes with a concluding section.

Apparatus and Experimental Procedure

The test rig used in the present experiments is shown in Fig. 6. This apparatus allowed control of both the injection pressure and

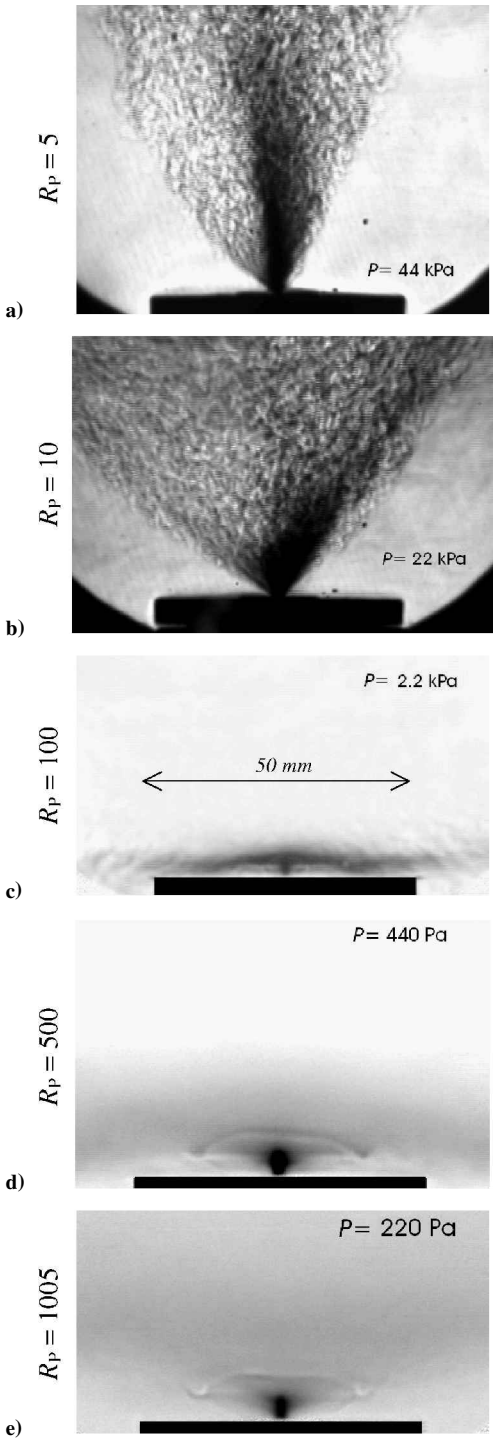

Fig. 3 Test series, nominal injection values $P_0 = 500$ kPa and $T_0 = 130°C$: from panel a to panel e, backpressure decreases (R_P increases). See Table 1 for measured data.

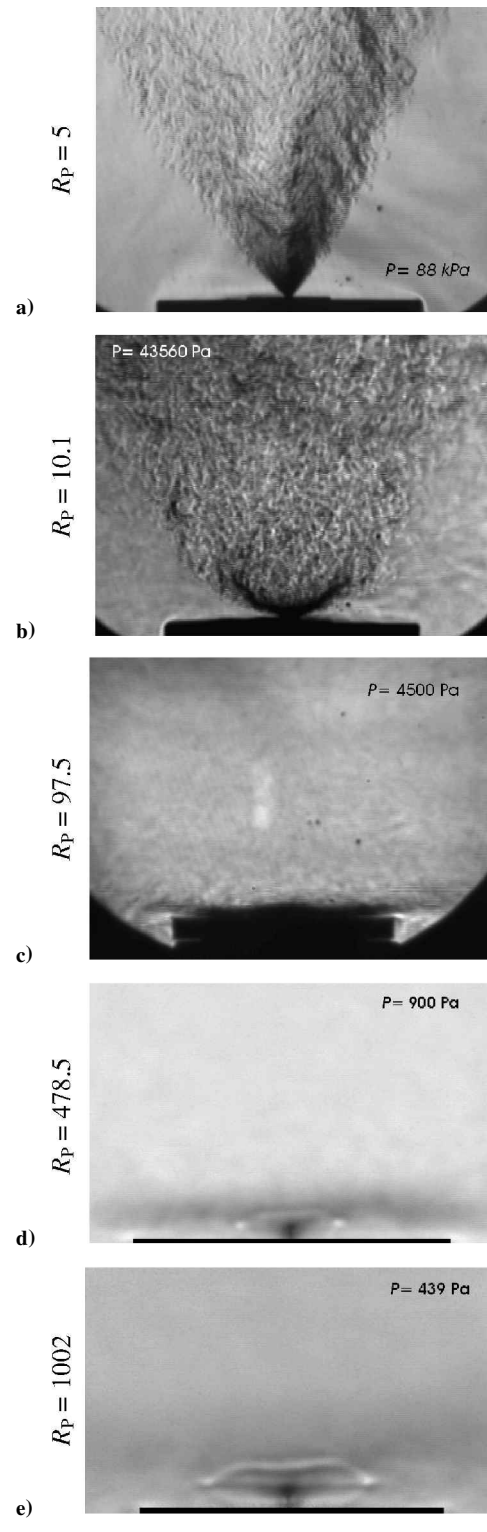

Fig. 4 Test series, nominal injection values $P_0 = 500$ kPa and $T_0 = 160°C$: from panel a to panel e, backpressure decreases (R_P increases). See Table 1 for measured data.

temperature of the testing liquid, as well as the backpressure. The main parts of the system are now described.

The flashing jet discharged into a low-pressure chamber of approximately 440ℓ, which was found to be large enough to carry out up to two tests of 3 cm^3 of liquid without significant pressure rise in the chamber for many of the experiments. A vacuum pump (Edwards Model E1M18) was used equipped with all other necessary pieces of equipment such as a vacuum trap condenser and instruments.

The main part of the injector was formed by a conical converging nozzle made of a regular machined carbon steel material having an exit section of 0.3 mm, an entrance diameter of 3 mm, and an 8-mm total length. The nozzle was housed in a hollow and annular chamber, where a heating fluid (oil) circulated in the hollow space enclosing a tube containing the test liquid. The heating oil circuit was formed by a pump, a reservoir, a valve, and a set of electrical heating coils, which allowed testing temperatures in the range of 20–300°C. The injection nozzle was normally obstructed by a sealing O-ring installed at the extremity of a rod, which was actuated by a pneumatic piston. The test liquid was supplied from a system formed by a small tube, whose extremity was connected to scaled glass tube, as shown in the schematics of Fig. 6. The liquid free surface was in contact with pressurized N_2 within the scaled glass tube, which kept the injection line pressure at the constant test pressure value set by a controlling valve installed in the N_2 line. An expansion chamber inserted in the N_2 line damped any line oscillations associated

with transients during the opening and closing stages. A test liquid reservoir supplied fresh liquid as necessary. Injection temperature was monitored by a thermocouple (type T, awg 30) positioned a few millimeters upstream of the nozzle entrance section and the pressure line was obtained using a pressure transducer (Kulite Model xte-190-100-A). Temperature and pressure signals were digitized using a regular 12-bit data acquisition system. The pressure transducer signal confirmed that the steady-state condition was achieved within a few milliseconds after the nozzle was opened. Readings of the mass flow rate were taken from the scaled glass tube. Figure 7 shows a schematic diagram of the mass flow rate measuring system. A set of light-emitting diodes (LEDs) was normally lit across the glass tube section and were sensed by a set of photodetectors, one for each LED, as shown in Fig. 7. As the testing liquid level lowered during the injection process, the light beams were blocked off one at a time, starting from the top. An electronic digital circuit combined all of the corresponding electrical signals into a single digital signal as shown in Fig. 7. This signal was then captured by the data acquisition system. The mass flow rate was then calculated for each time interval as the quotient $\rho \cdot \Delta V/\Delta t$, where ρ was the testing liquid density, ΔV was the volume displaced between signal steps, and Δt was the corresponding time interval.

The optical system was based on the classical schlieren method in the Z configuration. Parabolic mirrors were used to obtain a parallel light beam covering a 10-cm-diam circular region. It was found that a standard 40-W automotive light bulb was suitable as

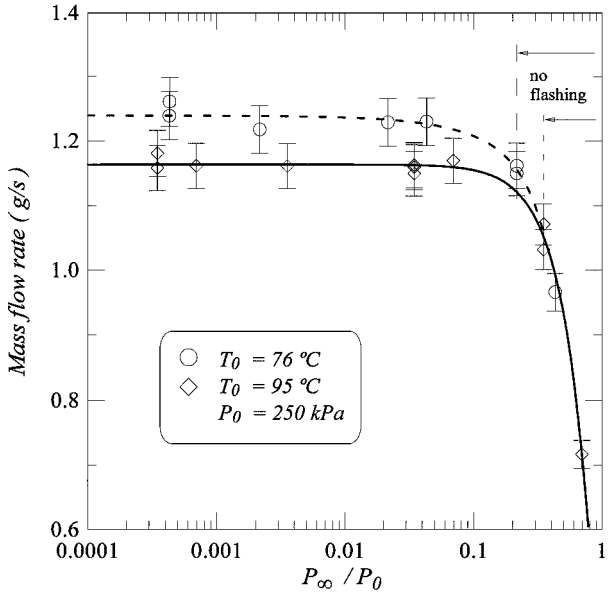

Fig. 5 Mass flow rate as a function of the backpressure to injection pressure ratio for two injection temperatures.

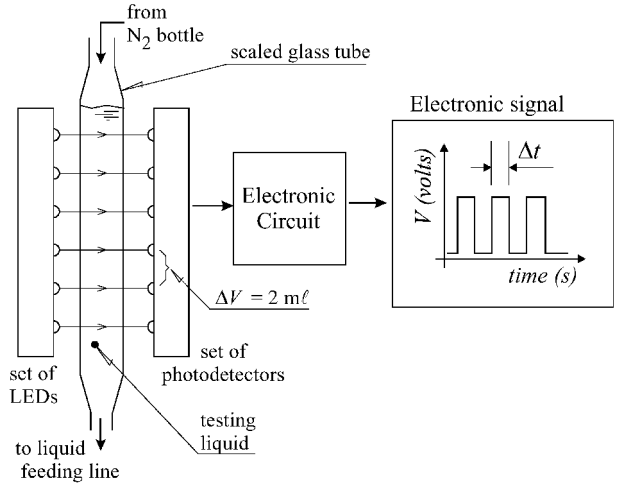

Fig. 7 Mass flow measuring system.

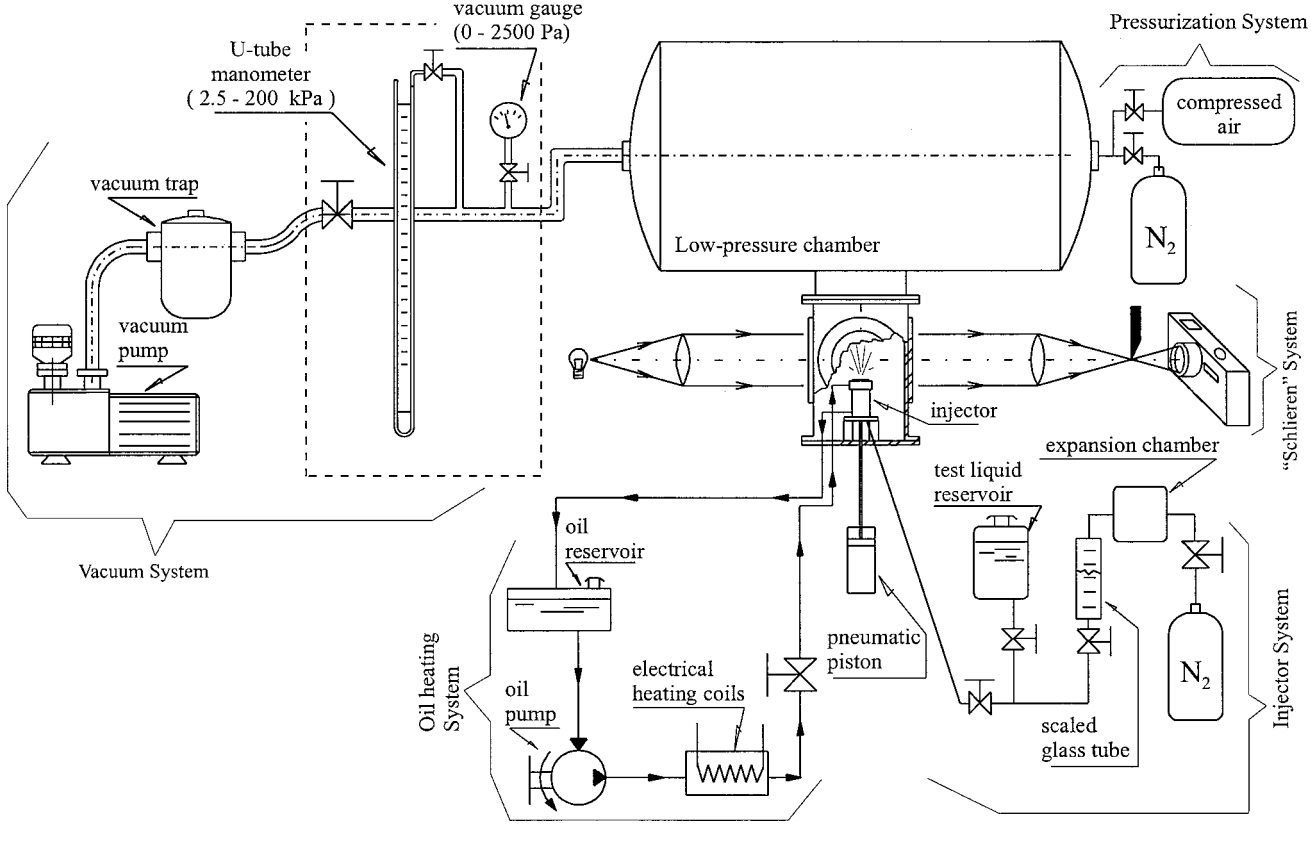

Fig. 6 General schematic diagram of the test facility.

a lighting source. A monochromatic charge-coupled device (CCD) camera (Coastar Model CV-M50) imaged the region of interest, obtaining frames at the regular rate of 30 frames/s. However, the electronic shutter aperture operated at a 0.1-ms time window. An image acquisition system (Data Translator Model DT-3152) captured the CCD images. Five frames were acquired during a typical injection process. One frame was taken just before the event started for subsequent image filtering purposes, and the remaining four frames were then obtained. A subtraction-type mathematical filter was later used to obtain sharper images.

A typical test started off by evacuating the low-pressure chamber. Vapors were condensed or frozen in the vacuum trap system installed in the vacuum line using liquid nitrogen. If the liquid injection line was empty, then it was also evacuated along with the low-pressure chamber by keeping the nozzle open. At the end of this stage, a low pressure (about 10 Pa) was achieved in the system. Next, the pneumatic piston was actuated closing off the nozzle, and the test liquid charge process started, filling the whole injection line. Fast opening/closing nozzle bleeding cycles were performed to ensure that no gases were trapped in the nozzle. In the sequence, the liquid line was pressurized with N_2 up to the testing pressure. The low-pressure chamber was partially filled with a cover gas (N_2), and a new vacuum cycle was carried out up to the testing backpressure value. The idea of using a cover gas was to avoid any potential hazardous situation because many fluids were and will be tested in future whose spontaneous ignition temperature may easily be reached.

After the test liquid had been charged into the system, the heating process took place. For this, the heating oil was set to circulate in the hollow chamber around the injector. Electrical power was supplied to the oil by a set of heating coils, and the delivered rate was controlled by a rheostat up to set value of the temperature of the test liquid. In this heating stage, a computer was monitoring both the injection pressure and temperature. Once all testing parameters have been set and checked, an experimental run could be performed, triggered by a computer signal. The same computer signal fed the system that triggered the pneumatic piston that opened the nozzle. Concurrently, the data acquisition system, as well as the image acquisition system, were also triggered. The whole event lasted about 5 s.

Figure 8 shows a typical set of signals obtained during a test. The top shows the injection pressure signal (249.6 kPa for this case). Relevant features are that the transients associated with the nozzle opening/closing events are quickly damped out, and, consequently, the injection pressure is kept constant during the test. The total test time is obtained from the electrical signal of a positioning sensor fixed on the moving piston-actuated rod that controls nozzle obstruction. Note that the nozzle opening/closing transients match exactly the positioning sensor signal as seen in Fig. 8. The third signal from the top comes from the mass flow rate system described earlier, which has also been shown in Fig. 7. Finally, the last signal proceeds from a thermocouple installed next to the nozzle entrance that monitors the liquid injection temperature.

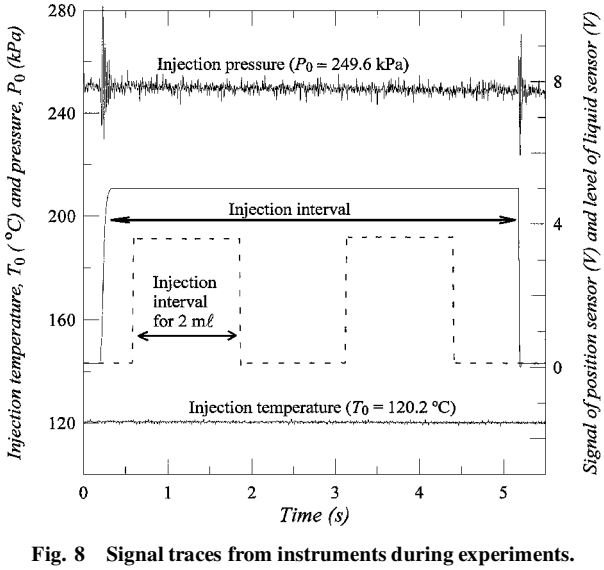

Fig. 8 Signal traces from instruments during experiments.

Experimental Results

Qualitative Descriptions of Still Pictures and Results

Figures 1–4 present selected still pictures obtained with the CCD camera imaging the schlieren system. All pictures have been mathematically filtered using a subtraction-type filter to get better quality photographs. Picture sequences are organized as follows. Figures 1 and 2 are for a 250-kPa injection pressure, and Figs. 3 and 4 are for a 500-kPa injection pressure. The liquid inlet temperature is constant, and nominal values are as follows: Fig. 1, $T = 76°C$; Fig. 2, $T = 130°C$; Fig. 3, $T = 130°C$; and Fig. 4, $T = 160°C$. Actual temperature values are indicate in Table 1. Pictures from Fig. 1a–4a to Fig. 1e–4e are for decreasing values of the low-pressure chamber (backpressure). A parameter R_P accounts for a systematically investigation of the backpressure influence. This parameter has been defined as the ratio of the vapor pressure at initial temperature to the backpressure value, that is, $R_P = P_v/P_\infty$. Relevant experimental data for each experiment are presented in Table 1. Other experimental conditions have also been investigated but are not presented for the sake of conciseness. Nevertheless, the general behavior was similar to that of these selected series.

For a pressure ratio R_P small, around 1.0 and lower, the liquid jet remains more or less intact and no evaporation has been observed, as indicated in Fig. 1a. This is the hydrodynamic regime, which does not interest us. As the backpressure decreases, that is, R_P increases, the expansion geometry and behavior of the emerging flashing liquid jet take different shapes and features. Experiments having the parameter R_P above unity to around 10 have indicated that the liquid jet shatters and opens up as it emerges from the nozzle. This is also a well-studied flashing regime in the context of atomization of liquid jets.[2] However, as R_P increases to around 100 and higher, a completely different expansion regime is observed. This paper is mostly concerned with the latter regime.

Table 1 Main experimental results

Run	P_0 ±1.8, kPa	T_0 ±1.2, °C	P_v, kPa	P_∞ ±0.06, kPa	R_P	$\dot{m}$ ±0.017, g/s	Figure	SW
45	251.3	76.5	54.7	108.07	0.5	0.966	1a	
43	250.7	75.7	53.7	54.04	1.0	1.150	1b	
27	250.1	76.2	54.3	54.04	1.0	1.162	——	
18	250.2	76.1	54.2	10.81	5.0	1.230	——	
17	249.1	76.2	54.3	5.40	10.0	1.229	1c	
16	251.5	76.7	54.9	0.54	102	1.218	1d	√
15	251.7	76.2	54.3	0.11	502	1.261	1e	√
42	251.8	76.6	54.8	0.11	507	1.239	——	√[a]
23	252.6	129.8	212.8	43.82	4.9	0.919	2a	
26	265.7	129.4	210.7	21.91	9.6	1.032	——	
22	249.6	130.7	217.5	21.91	9.9	1.024	2b	
21	251.3	131.1	219.6	2.19	100	0.996	2c	
14	250.0	132.8	228.8	0.46	498	0.877	——	√[a]
25	257.1	130.9	218.6	0.44	499	0.880	2d	√
24	256.2	130.2	214.9	0.22	981	0.863	2e	√
19	250.6	131.8	223.4	0.22	1020	0.714	——	√[a]
38	500.7	131.0	219.1	43.82	5.0	1.605	3a	
37	499.2	131.1	219.6	21.91	10.0	1.555	3b	
36	501.1	131.0	219.1	2.19	100	1.574	3c	√
40	500.0	131.0	219.1	0.44	500	1.517	3d	√
35	501.7	131.4	221.2	0.44	505	1.515	——	
33	500.5	131.2	220.2	0.22	1005	1.451	3e	√
32	501.5	161.9	439.9	88.17	5.0	1.352	4a	
31	501.9	162.6	446.4	44.09	10.1	1.260	4b	
30	502.5	160.8	430.0	4.41	98	1.155	4c	
29	504.1	159.9	421.9	0.88	478	1.131	4d	√
28	543.3	161.9	439.9	0.44	998	1.185	——	√[a]
34	502.1	162.1	441.8	0.44	1002	1.105	4e	√
55	500.9	162.0	440.0	0.40	1100	0.964	9a	√

[a]Not shown.

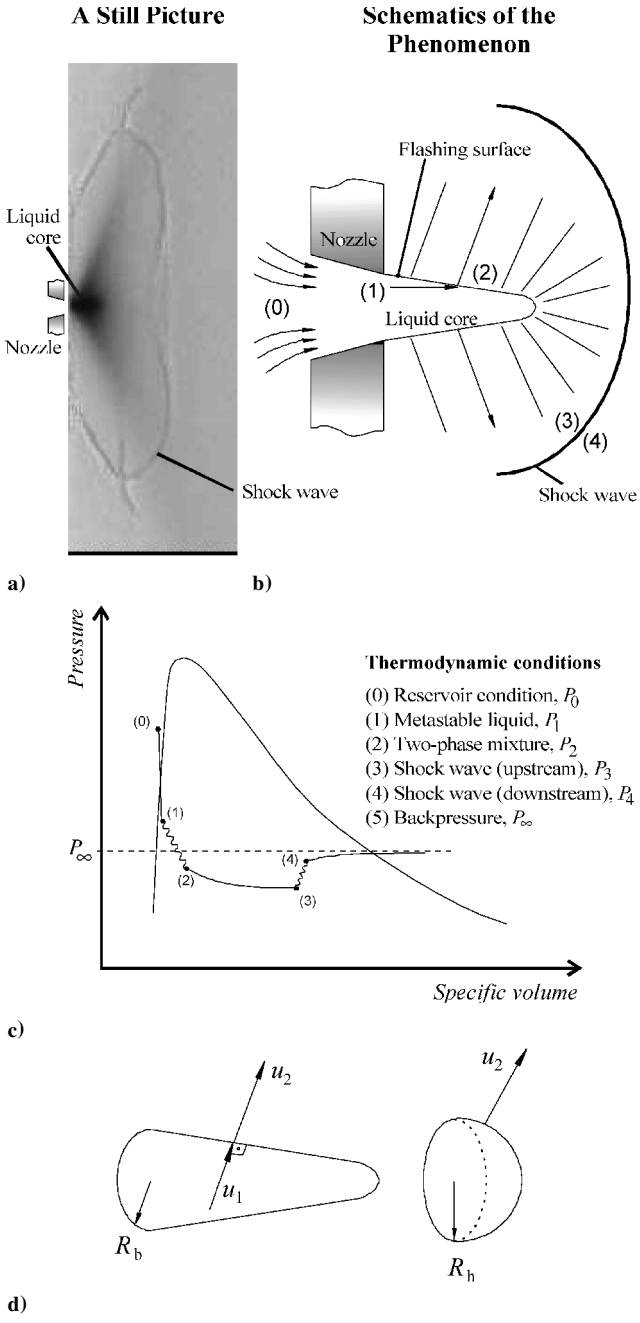

Fig. 9 General behavior of a flashing liquid jet: a) still picture (run 55; see Table 1 for details) of flashing liquid jet showing metastable liquid core and the shock wave structure, b) schematic of the jet stressing the main thermodynamic states, which are also indicated in c) the P–v plane, and d) equivalence between the original metastable core (which resembles a cone) and one-dimensional hemispherical geometry.

Concentrating on cases of $R_P \approx 100$ and above, it can clearly be observed that a shock wave structure appears coupled with the flashing jet. This shock wave does possess an irregular geometry, whose frontal portion resembles spheroidal surfaces in some situations and ellipsoidal in others. In other circumstances, the lower portion of the shock wave seems to be flat. The photographs in Figs. 1–4 also indicate that in some experiments a shock wave reflection is seen somewhere in the average shock wave plane (also see Fig. 9). As a general rule, an average or representative diameter of this shock wave increases as the backpressure decreases (higher R_P). The presence of a shock wave structure enveloping the flashing liquid jet implies that 1) supersonic velocities are present, 2) the supersonic expansion occurs in all directions, and, even more intriguing, 3) measurements of the mass flow rate point out that above a certain of R_P value the discharging liquid jet gets choked. The R_P choking threshold depends on the injection pressure and temperature, as well as the thermodynamic properties of the testing liquid, as it will be discussed later. Finally, the central liquid core is seen somewhat blurred, which certainly is a consequence of the high speeds present during the flashing. However, it is clear from the photographs that the liquid central core does extinguish some diameters downstream of the nozzle exit section as the result of the intense liquid evaporation process. A proper discussion of this topic is delayed to the numerical solution analysis section.

Experimental Data

Table 1 presents the main experimental results. The first column refers to the experiment run number. Columns 2 and 3 show the injection pressure P_0 and temperature T_0, respectively. The corresponding vapor pressure at the injection temperature is P_v. P_∞ is the low-pressure chamber pressure. R_P is the pressure ratio parameter seen in the next column, which is followed by the measured mass flow rate $\dot{m}$. The last two columns indicate which figures the data are valid for, and an observation mark ($\surd$) notes the cases where a shock wave (SW) appears in the corresponding figure. The international system of units has been used. Measured and calculated uncertainties are also indicated.

One-Dimensional Model

General Thermodynamic Behavior: One-Dimensional Hypothesis

Figure 9a shows a still picture stressing the main peculiarities of a highly expanded flashing liquid jet and the main associated phenomena. As shown in Fig. 9b, compressed liquid is initially in the reservoir at a thermodynamic state 0. The first expansion process ($0 \rightarrow 1$) that the liquid undergoes occurs inside the nozzle, which leads to the metastable state 1 at the exit section. By assumption, the metastable liquid state 1 is uniform and constant across the nozzle exit section down to the entire liquid core. As also inferred from the experimental observations, the sudden phase transition ($1 \rightarrow 2$) occurs on the liquid core surface through an evaporation wave, a phenomenon well studied by Simões-Moreira and Shepherd.[11] The main characteristics of an evaporation wave are as follows: 1) The evaporation wave is a narrow and observable region that envelopes the evaporation front; 2) in an evaporation wave, the metastable liquid is transformed into a high-speed two-phase flow; and 3) at the extreme pressure ratio conditions (high R_P) tested in the present experiments, the normal velocity component of the two-phase flow is sonic in relation to the evaporation wave, as will be discussed later. Also, as an evaporation wave traverses a metastable liquid, the fluid pressure and, of course, the temperature decrease as a consequence of the sudden evaporation process.[11] Next, the freshly formed sonic two-phase flow expands freely from the evaporation wave interface to increasing supersonic velocities, which comprises the expansion process ($2 \rightarrow 3$). Finally, the supersonic expansion process terminates with a shock wave ($3 \rightarrow 4$) to match the fluid pressure with the reservoir pressure in the far field downstream of the shock wave. All processes and thermodynamic states are also shown in the pressure–specific volume plane in Fig. 9c.

As can be seen in Figs. 1–4, both the metastable liquid jet and the SW geometry possess at least two-dimensional features. Consequently, the complete solution for the present cases for which a radial symmetry holds requires a computational code to solve this problem. Evidently, other more complex boundary conditions, such as internal walls of expansion valves passages, will also demand considerable computation efforts. However, to obtain a preliminary physical model of the several phenomena presented in the flashing liquid jet, it is possible to assume a one-dimensional solution in the radial direction by making some assumptions.

First, the actual liquid core should take the shape of a cone, if a constant evaporation rate is assumed along with constant and uniform properties of the metastable liquid within the liquid core. This is the cone of evaporation. Still pictures[8] also reveal that the two-phase mixture expands in an almost 90-deg angle to the main axial direction. When these flow characteristics are considered, it is proposed to carry out a one-dimensional flow calculation in the radial

Table 2 Numerical results of one-dimensional solution

					C–J condition					Uspstream SW						Downstream SW						Dimensions		
Run	P_0, kPa	P_∞, kPa	T_1, °C	P_1, kPa	T_2, °C	P_2, kPa	x_2	u_2, m/s	v_2, m³/kg	T_3, °C	P_3, kPa	x_3	u_3, m/s	v_3, m³/kg	M_3	T_4, °C	P_4, kPa	x_4	u_4, m/s	v_4, m³/kg	M_4	r_1, mm	r_2, mm	r_{sw}, mm
16	251.5	0.54	76.7	15.5	31.3	8.88	30.4	73.6	0.816	−48.9	0.043	59.8	326.0	22.7	3.3	−20.8	0.45	60.9	34.0	25.0	0.31	6.5	7.6	11.6
15	251.7	0.11	76.2	1.76	−10.6	0.90	53.9	102.3	12.20	−63.2	0.010	66.8	326.4	1000.0	3.2	−39.6	0.10	70.5	37.4	100.0	0.34	14.0	10.1	25.1
21	251.3	2.19	131.1	79.2	72.1	44.0	44.8	97.9	0.271	−33.3	0.170	78.9	416.3	81.9	3.2	2.6	2.55	87.2	45.8	9.1	0.33	3.5	2.6	5.6
24	256.2	0.22	130.2	127.2	90.4	78.4	31.8	74.8	0.113	−57.3	0.019	80.8	485.0	666.7	4.2	−25.2	0.34	——[a]	41.9	50.0	0.36	12.2	6.8	13.8
36	501.1	2.19	131.0	71.3	70.0	40.8	46.2	95.9	0.300	−33.2	0.172	79.1	413.9	82.0	3.2	2.5	2.03	87.2	46.0	9.1	0.33	4.4	4.3	7.0
40	500.0	0.44	131.0	100.7	81.3	59.4	38.7	86.3	0.179	−54.6	0.024	81.3	477.3	526.3	4.1	−21.7	0.42	99.2	41.5	50.1	0.29	13.4	7.2	16.3
33	500.5	0.22	131.2	135.1	92.6	84.0	31.1	73.3	0.103	−56.0	0.022	81.0	484.2	588.2	4.2	−23.3	0.38	——[a]	42.0	49.9	0.36	13.4	7.4	16.9
30	502.5	4.41	160.8	257.4	116.2	160.8	39.7	84.1	0.071	−27.8	0.268	89.3	479.1	62.9	3.6	21.9	3.57	——[a]	45.9	5.9	0.31	——[b]	——[b]	4.9
29	504.1	0.88	159.9	269.6	119.0	172.0	36.7	79.2	0.062	−50.6	0.037	90.3	537.9	400.9	4.4	19.4	0.71	——[a]	40.6	33.3	0.27	7.6	4.5	11.5
34	502.1	0.44	162.1	277.1	120.1	175.7	38.1	81.4	0.063	−58.7	0.016	90.9	564.5	909.1	4.4	21.7	0.36	——[a]	38.9	50.1	0.26	10.0	5.5	16.5
A6[c]	2397	5.73	204.0	450.4	136.8	263.3	67.1	119.5	0.074	−27.9	0.266	98.5	576.3	69.9	4.2	71.4	4.64	——[a]	44.4	5.6	0.27	25.0	15.0	20.4
A7[c]	2338	8.25	200.0	435.9	135.7	256.9	63.7	115.2	0.072	−21.0	0.440	99.8	545.9	44.1	3.8	69.9	6.63	——[a]	46.7	3.7	0.29	14.0	11.0	16.6
A8[c]	2293	9.87	200.0	426.4	134.1	247.7	64.8	118.2	0.076	−14.6	0.552	——[a]	538.2	35.7	3.8	73.6	7.95	——[a]	47.9	3.2	0.29	13.0	12.0	15.0

[a]Complete evaporation. [b]Not distinguishible. [c]Reference 8, experiment, 3 Nov. 1994, runs 6, 7, and 8.

direction. To achieve this, the cone of evaporation is approximated by a hemisphere named the hemisphere of evaporation as schematically shown in Fig. 9d.

Second, the equivalence between the hemisphere and the cone is obtained by defining a hemisphere radius R_h, such that the same mass flow rate traverses both the hemisphere and the nozzle to maintain the original problem, which is mass flow rate dependent. Also, for consistency with the mass conservation law, the normal velocity component of the two-phase flow of the original problem becomes the radial component in the one-dimensional problem. In doing so, the following equation is obtained that defines the radius of the hemisphere:

$$R_h = \sqrt{\dot{m} \cdot v_2 / 2\pi u_2} \tag{1}$$

where $\dot{m}$ is the mass flow rate, v_2 is downstream specific volume, and u_2 is the downstream normal component.

Figure 9d shows the equivalence between the original problem and the one-dimensional hemispherical problem. Other authors[7] have assumed an expansion in the direction radial to the jet centerline. This paper presents an expansion in the regular radial direction, that is, the radial direction taken in relationship to the center point of the nozzle exit section.

Another point that deserves attention is the estimation of the metastable liquid state. Accordingly, it can be assumed that during the expansion process within the nozzle the liquid undergoes a nearly isothermal process[3] and, therefore, the metastable liquid temperature is approximated by the injection temperature, that is, $T_1 \approx T_0$. This assumption allows one to estimate the metastable pressure P_1 using the discharge coefficient formula for orifices, whose expression is

$$P_1 = P_0 - \dot{m}^2 v_1 \big/ 2A^2 C_D^2 \tag{2}$$

where A is the nozzle exit section area, $C_D = 0.94 \pm 0.02$ is the discharge coefficient for the nozzle used in this experiment, whose value was found experimentally in a standard procedure. As a first solution, it was assumed that the metastable specific volume v_1 was taken to be the same as the saturation specific liquid volume at the injection temperature T_0. The fifth column in Table 2 shows the estimated metastable pressure for the cases of interest.

Evaporation Wave Jump Equations

After the estimation of the metastable liquid state by the procedure described earlier, the next step is to solve the evaporation wave problem, that is, to calculate the jump properties across the metastable liquid two-phase interface. This flow discontinuity corresponds to the process (1 → 2) in Fig. 9b. To achieve this, the one-dimensional jump equations are solved.[3,7,11,13] The mass, momentum, and energy conservation equations are

$$[J] = [u/v] = 0 \tag{3}$$

$$[P + uJ] = 0 \tag{4}$$

$$[h + u^2/2] = 0 \tag{5}$$

where the square brackets indicate a jump in the enclosed value, that is, $[f] = f_2 - f_1$ and where v is the specific volume, u is the radial fluid velocity, P is the pressure, h is the specific enthalpy, and J is the superficial mass flux, that is, the mass flow rate per unit of area. Subscripts 1 and 2 are for upstream (metastable liquid) and downstream (two-phase mixture) states, respectively. For a given metastable liquid upstream state 1, there exists a corresponding singular solution for low downstream pressure values. This solution is the C–J condition.[3,7,11,13] With the C–J solution, the two-phase flow becomes sonic in relation to the evaporation front, that is, u_2 is sonic. The preceding equations are valid for steady state, which means that the metastable liquid core is stationary in relation to a laboratory frame. The one-dimensional approach neglects the details of the actual evaporation wave geometry. In reality, the experiments indicated that the actual interface is oblique in relation to the main fluid metastable fluid velocity u_1, which originated a study[13] regarding geometrical relationships between upstream and downstream states and velocities. However, for the sake of the present radial one-dimensional theory, the original normal velocity component become the radial velocity in the present one-dimensional modeling context.

Expansion Region and SW Position

After the metastable liquid has undergone a sudden evaporation through an evaporation wave, the sonic state 2, or the C–J solution is reached at the downstream side of the evaporation wave. The two-phase mixture continues to expand further. As a consequence, the mixture increases its velocity to higher Mach numbers, while the pressure, temperature, and density fall substantially, as occurs in one-dimensional supersonic flow acceleration in an ordinary gas or vapor. The supersonic expansion process can be modeled considering the three conservation equations in one-dimensional spherical coordinate (r dependence only):

$$\frac{\mathrm{d}\dot{m}}{\mathrm{d}r} = \frac{\mathrm{d}}{\mathrm{d}r}\left(\frac{Au}{v}\right) = 0 \tag{6}$$

$$\frac{\mathrm{d}(u\dot{m})}{\mathrm{d}r} + A\frac{\mathrm{d}P}{\mathrm{d}r} = 0 \tag{7}$$

$$\frac{\mathrm{d}h_0}{\mathrm{d}r} = 0 \tag{8}$$

where $A = 2\pi R^2$ is the hemisphere area, h_0 is the total specific enthalpy, and all of the remaining magnitudes have already been defined.

The expansion process continues until a hemispherical SW is eventually formed at a position such that a pressure matching condition is established in the far field. Because of the radial nature of the flow, pressure matching is obtained by equating the fluid pressure in the far field downstream of the SW (state 5) with the backpressure P_∞, that is,

$$P_5 = P_\infty \tag{9}$$

In a broader sense, the standard jump equations for a regular SW are solved (refer to a text book on compressible flow, for instance) with the matching condition given by Eq. (9). Of course, the pressure downstream of the shock wave increases from the value P_4 as the fluid expands (now in the subsonic regime) to a far-field value P_5, so that the backpressure P_∞ is reached. The far-field position is taken as a location such that the kinetic energy is negligible.

Mach numbers for the two-phase flow were calculated by the standard definition, that is, the ratio of the local fluid velocity to the speed of sound C. To avoid difficulties that are usually associated with establishing the speed of sound in two-phase flow, the isentropic definition was used:

$$C^2 = -v^2\left(\frac{\partial P}{\partial v}\right)_s \tag{10}$$

where s is the specific entropy. The partial differential was numerically obtained whenever necessary by using a simple forward difference scheme over an isentropic line.

Numerical Solution and Analyses

Numerical Solution Procedure

The problem was solved using the code Showphast 1D. This code was developed by the first author and modified by the third author. The solution procedure is described as follows:

1) Discharge coefficient C_D, mass flow rate $\dot{m}$, and initial conditions P_0 and T_0 are supplied as input data along with the nozzle exit section area. With these data, the metastable pressure P_1 is calculated from Eq. (2). It is also assumed that the liquid injection temperature T_0 is kept constant and that the specific volume is equal to the saturation value at T_0 down to the exit nozzle section.

2) The jump equations (3–5) are solved[11,13] next by assuming the singular C–J solution.[13] The C–J solution also means that the two-phase flow is sonic ($M_2 = 1$) in relation to the evaporation front. This condition corresponds to thermodynamic state 2 in Fig. 9b.

3) The hemisphere radius R_h of the metastable liquid is calculated next according to Eq. (1).

4) The expansion process is obtained as a function of the radial position r by using a downstream marching scheme to integrate the conservation equations (6–8), with the initial condition given by the C–J solution described in step 3.

5) At each new r step, the standard jump equations for an ordinary shock wave are solved. Next, the fluid downstream of the shock wave is allowed to expand to the far field. If the matching condition [Eq. (9)] is satisfied, then the location of the hemispherical SW has been established in that particular radial location. Otherwise, the marching process continues downstream to next r step.

Results of Numerical Solution and Analyses

Table 2 presents relevant results of the numerical solution. The first column displays the experiment run identification. The next three columns present the main experimental conditions, which are the injection pressure P_0, the reservoir pressure P_∞, and the metastable temperature T_1, which is taken as the same as the injection temperature T_0. The metastable pressure P_1 is also shown, which was estimated using Eq. (2). Other corresponding measured data are provided in Table 1 for each run.

With regard to Table 2, the set of columns labeled C–J condition refer to the downstream states of the one-dimensional solution of the evaporation wave [Eqs. (3–5)]. All magnitudes have already been defined except x, which is the mass vapor quality. The next set of columns refers to the upstream condition of the SW, whereas the following set of columns, labeled downstream SW, presents relevant thermodynamic properties downstream of the SW. Columns r_1 and r_2 refer to two representative lengths of the observed SWs as illustrated in a sample still photograph shown in Fig. 10. Finally, the last column refers to the one-dimensional model results regarding the radial position where the SW is formed, r_{SW}. Calculated Mach numbers are also provided in Table 2 for the fluid upstream, M_3, and downstream, M_4, of the SW. Mach numbers for the C–J condition is sonic, $M_2 = 1$, and have been omitted.

Finally, some vapor quality downstream SW x_4 are not shown in Table 2. This is because the two-phase mixture has completely evaporated after shock. Complete adiabatic evaporation is a possibility in retrograde fluids,[7,10,12] such as iso-octane. Three selected experimental results obtained by Athans[8] are also shown in Table 2, and they were chosen among many others because of the corresponding still photographs allowed estimation of SW dimensions.

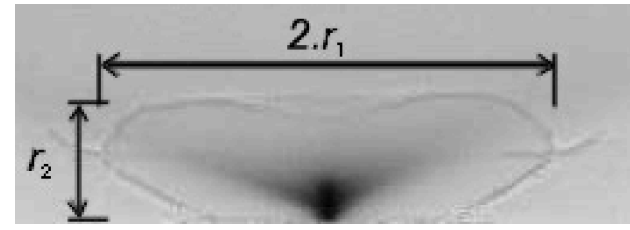

Fig. 10 Representative lengths of a SW.

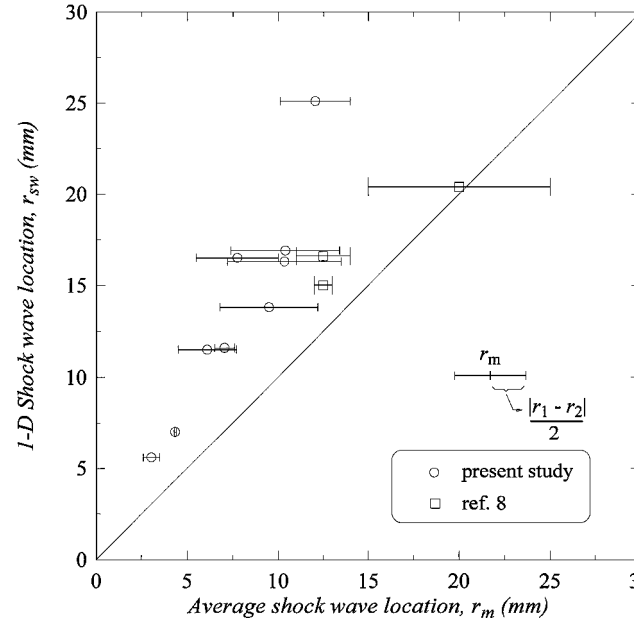

Fig. 11 Average representative length compared with hemispherical SW radius.

SW Position

For a given injection pressure and temperature, the still photographs indicated that the shock wave size increases with decreasing backpressure. This finding also means that the location where the SW structure is formed is each time farther away from the nozzle exit as the backpressure is lowered, which can clearly be seen in each one of the isothermal testing series of Figs. 1–4. Consequently, the representative lengths r_1 and r_2 decrease with increasing reservoir pressure, as indicated in Table 2. The problem of the SW location is well captured by the one-dimensional model, as indicated in the last columns of Table 2; compare r_{SW} with r_1 and r_2. Figure 11 shows a graph comparing the two representative lengths and its average value with the hemispherical SW radius r_{SW} for the several cases indicated in Table 2. The average representative length r_m is the mathematical

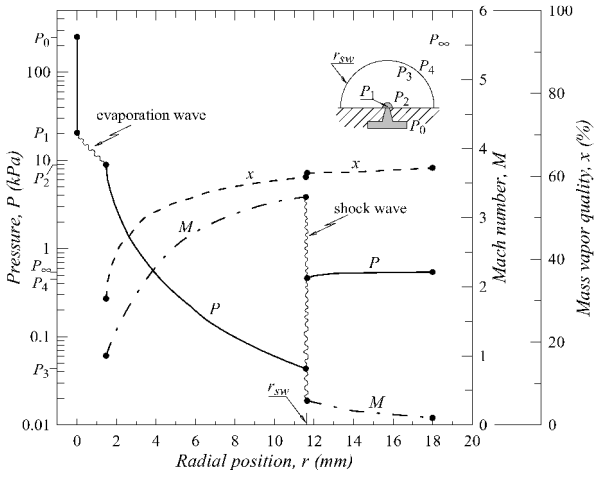

Fig. 12 Pressure, mass vapor quality, and Mach number distribution as a function of the radial position obtained from the one-dimensional modeling (run 16; see Tables 1 and 2 for further details).

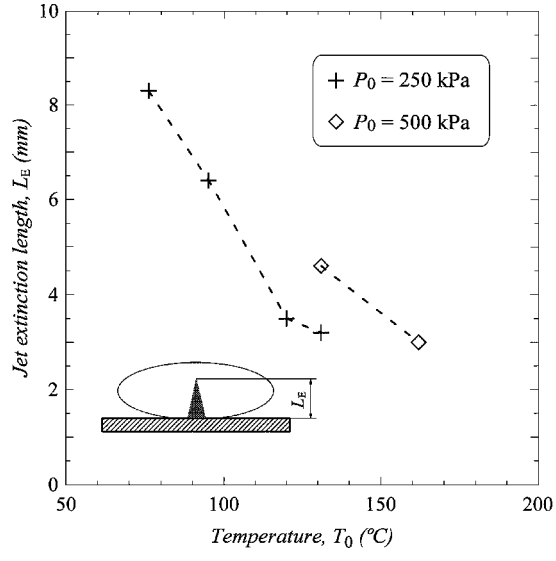

Fig. 13 Extinction length of the metastable liquid jet as function of the injection temperature and pressure.

average of r_1 and r_2. Also, r_1 and r_2 are shown in Fig. 11 as error bars around the average radius r_m. The Fig. 11 graph also shows that, in general, the one-dimensional model overestimates the SW position. In addition, as the backpressure decreases, the average SW location moves forward.

Figure 12 shows three different graphs stressing property variation throughout the whole flashing process as a function of the radial position for a studied case. The pressure distribution behavior can be understood as follows. Initially, the liquid is at injection pressure P_0. As it expands within the nozzle, it reaches the metastable pressure P_1 at the exit section. An evaporation wave transforms the metastable liquid into a sonic two-phase flow at the C–J condition and pressure P_2. The mixture expands to increasing Mach numbers, while the pressure decreases. The supersonic expansion terminates with a SW, which brings the Mach number down to subsonic values and increases the pressure to P_4. Finally, the fluid expands in the subsonic regime to a far-field pressure until matching with the backpressure P_∞ is accomplished. The case studied remained entirely within the saturation dome, except for states 0 and 1. Other graphs in Fig. 12 show the evolution of the Mach number and the mass vapor quality.

Figure 13 shows the measured extinction length L_E of the metastable liquid jet as function of temperature for the two tested injection pressure. The extinction length is also shown in the Fig. 13 diagram on the left-bottom corner. Figure 13 clearly shows that, for a given injection pressure, the extinction length decreases significantly with increasing injection temperature. This behavior is certainly associated with that higher evaporation rates should occur in connection with increasing temperature. Figure 5 shows the mass flow rate as a function of the backpressure to injection pressure ratio for two injection temperatures. It can be seen that, below a certain pressure ratio threshold, the mass flow rate becomes independent of the pressure ratio, which indicates that a choking condition has been reached, which corroborates the assumption made in this paper.

Conclusions

Flashing liquid jets have been observed in small short converging nozzles. Schlieren still pictures have shown that for a low-pressure chamber (R_P around 100 and higher for the cases studied) the flashing jet has special features. The present authors, as well as previous authors,[6,8] have observed experimentally a liquid core issuing from the nozzle, which implies that no internal nucleation has been observed and that the phase transition occurs outside the nozzle. Estimations have shown that a very high degree of metastability is reached during the experiments. This can be verified by comparing a metastable pressure value P_1 from Table 2 with the corresponding vapor pressure P_v (Table 1) for a specific run. The experiments indicate that there exists a liquid core from which a two-phase mixture derives. The sudden phase transition takes place in the interfacial region surrounding this liquid core. This interfacial region is known as an evaporation wave.[7,11,13] For these experiments, the C–J solution has been applied to model this evaporation process. A closer examination of still pictures[8] shows that the evaporation region is slanted to the main fluid velocity (axial). A proper discussion of the implications of an oblique evaporation wave has been discussed previously.[13] The study indicates that the main flow velocity undergoes a drastic change in direction. Originally, the flow was in the axial direction and, as it goes through evaporation in the interfacial region, it turns away from the interface and spreads out, which is quite consistent with the photographs shown in this work and in previous studies.[8] The C–J solution has been applied, which means that the two-phase flow leaves the interface that encloses the metastable liquid core at the local speed of sound. This sonic two-phase flow expands further, reaching supersonic velocities. The expansion terminates with a complex SW geometry, so that the matching reservoir condition is achieved, that is, total pressure after the SW equalizes the reservoir pressure. The one-dimensional model consistently anticipates the SW position.

Acknowledgments

The authors would like to acknowledge the financial support for this project from Fundação de Amparo à Pesquisa do Estado de São Paulo (FAPESP) (Brazil) and Wagner de Rossi and CPML personnel from the Energetic and Nuclear Research Institute for making the pinholes. The first author thanks the Conselho Nacional de Desenvolvimento Científico e Tecnológico for personal support. The second and third authors also thank FAPESP for personal support.

References

[1]Reid, R. C., "Possible Mechanism for Pressurized-Liquid Tank Explosions or BLEVE's," *Science*, Vol. 23, No. 4386, 1979, pp. 1263–1265.

[2]Oza, R. D., and Sinnamon, J. F., "An Experimental and Analytical Study of Flash-Boiling Fuel Injection," International Congress and Exposition, Society of Automotive Engineers, SAE Paper 830590, 1983.

[3]Simões-Moreira, J. R., and Bullard, C., "Pressure Drop and Flashing Mechanisms in Expansion Devices," *International Journal of Refrigeration* (submitted for publication).

[4]Edwards, A. R., and O'Brien, T. P., "Studies of Phenomena Connected with Depressurization of Water Reactors," *Journal of the British Nuclear Energy Society*, Vol. 9, No. 2, 1970, pp. 125–135.

[5]Wildgen, A., and Straub, J., "An Investigation of Boiling Phenomena in Superheated Free Jets," *Proceedings of the Eighth International Heat*

Transfer Conference, Vol. 5, American Society of Mechanical Engineers, Fairfield, NJ, 1986, pp. 2251–2256.

[6]Reitz, R. D., "A Photographic Study of Flash-Boiling Atomization," *Aerosol Science and Technology*, Vol. 12, No. 3, 1990, pp. 561–569.

[7]Kurschat, T., Chaves, H., and Meier, G. E. A., "Complete Adiabatic Evaporation of Highly Superheated Jets," *Journal of Fluid Mechanics*, Vol. 236, 1992, pp. 43–58.

[8]Athans, R. E., "The Rapid Expansion of Near-Critical Retrograde Fluid," Ph.D. Dissertation, Mechanical Engineering Dept., Rensselaer Polytechnic Inst., Troy, NY, 1995.

[9]Vieira, M. M., Guimarães, M. S., and Simões-Moreira, J. R., "An Experimental Study of Flashing Jets," *ENCIT 2000—Brazilian Congress on Thermal Engineering and Science*, Brazil, 2000, Paper S16P18 (in Portuguese).

[10]Simões-Moreira, J. R., McCahan, S., and Shepherd, J. E., "Complete Evaporation Waves," Fluids Engineering Conf., American Society of Mechanical Engineers, ASME Paper 93-FE-7, 1993.

[11]Simões-Moreira, J. R., and Shepherd, J. E., "Evaporation Waves in Superheated Dodecane," *Journal of Fluid Mechanics*, Vol. 382, 1999, pp. 63–68.

[12]Thompson, P. A., and Sullivan, D. A., "On the Possibility of Complete Condensation Shock Waves in Retrograde Fluids," *Journal of Fluid Mechanics*, Vol. 70, 1975, pp. 639–49.

[13]Simões-Moreira, J. R., "Oblique Evaporation Waves," *Shock Waves*, Vol. 10, No. 4, 2000, pp. 229–234.